Journal of Sound and Vibration (1999) **220**(3), 517–539
Article No. jsvi.1998.1962, available online at http://www.idealibrary.com on IDEAL

THE IN-PLANE VIBRATION OF THIN RINGS WITH IN-PLANE PROFILE VARIATIONS PART II: APPLICATION TO NOMINALLY CIRCULAR RINGS

C. H. J. Fox, R. S. Hwang and S. McWilliam

Department of Mechanical Engineering, University of Nottingham, University Park, Nottingham NG7 2RD, England

(*Received* 24 *February* 1998, *and in final form* 7 *September* 1998)

Geometric profile variations always exist in nominally circular rings due to limitations in the manufacturing processes. Such profile variations are known to lead to frequency splitting between pairs of modes which are degenerate in a perfect ring. In this paper, the effects of circumferential profile variations on the in-plane vibration characteristics of such rings are studied using a numerical method. The inner and outer ring surfaces are described in a very general way by Fourier series and the Rayleigh–Ritz method is used to obtain the natural frequencies and mode shapes. Results are presented for a number of example cases which include single- and multiple-harmonic variations in profile. The relationship between the patterns of frequency splitting and the harmonic content of the ring profile is investigated and the most important causes of frequency splitting are identified.

1. INTRODUCTION

A companion paper [1] presented a theoretical approach for calculating the natural frequencies and mode shapes for the in-plane vibration of rings with circumferentially variable, in-plane radius of curvature of the bounding surfaces. Fourier series were used to define the inner and outer surfaces of the ring, thus permitting any single valued closed ring shape to be modelled in a general way with any required degree of accuracy. The true mid-surface of the ring was then found from the inner and outer surface profiles using an iterative numerical procedure, and the Rayleigh–Ritz method was used to determine the natural frequencies and mode shapes.

The current paper presents a number of application examples of the theory given in reference [1]. These are based on rings which are notionally circular in shape, but which deviate from perfect axial symmetry in a number of ways. One aim of the work reported here is to gain an improved, quantitative understanding of the effects of departures from true circularity caused by limitations in manufacturing processes. This is particularly relevant to applications such as vibratory gyroscopes

0022–460X/99/080517 + 23 $30.00/0

[2, 3], where the frequency splitting caused by imperfection is vitally important and must be controlled to within fine limits of the order of 0·01% (100 ppm) or better. Therefore, there is a specific need to understand the effects of small profile variations (i.e., departure from circularity is small compared to the mean radial thickness of the ring) and results are presented for this situation. However, the method of analysis is equally applicable to cases where the departure from circularity is large and a number of such cases are also considered, including regular polygons.

As mentioned above, the solution method used [1] relies on decomposing the inner and outer surface profiles of the ring as Fourier series. This has a number of advantages. First, the Fourier series is the most natural way to describe any continuous, periodic closed structure, of which a ring is perhaps the most obvious example. Second, when discussing departure from circularity (imperfection), there is a need to quantify the effect in a way which can be usefully interpreted in the context of its effect on ring vibration and the Fourier coefficients provide a convenient way to do this. Furthermore, modern metrology equipment for measuring circular forms often provides the required Fourier series description.

The Fourier series description of the ring profiles leads naturally to the idea of the profile-spectrum of the ring shape. The way in which individual harmonics in the profile-spectrum affect ring vibration modes of a given harmonic number is of particular interest because there is the prospect that these can be controlled during the manufacturing process.

Many papers have been published on the subject of the in-plane vibrations of circular rings, the great majority of which are restricted to perfectly circular rings. Relatively few papers have been published on the effects of departure from perfection and the most important of these are briefly reviewed below. Reference [4] presented an investigation of frequency splitting in a thin circular ring due to equal masses which were assumed to be attached to the ring at the vertices of an inscribed regular nth order polygon. A perturbation method and Group Theory were used to obtain selection rules for the splitting of doublets. The rules predicted when splitting would occur, but did not indicate the magnitude of the frequency splits. An experimental study, which verified the main theoretical predictions, was presented in reference [5].

Reference [6] described theoretical perturbation studies and experimental measurements of the radial vibrations of eccentric rings. Frequency splitting due to eccentricity was predicted to be small for most modes of vibration and the experimental measurements supported the theoretical predictions.

Reference [7] presented an analysis of the vibration of an eccentric, thin walled cylinder. It was assumed *a priori* that the mid-surface was circular and Fourier series were used to represent the circumferential variation of the wall thickness. The assumption of a circular mid-surface is not strictly valid in general and will only be a valid approximation for small values of eccentricity. Agreement between theoretical predicted and measured natural frequencies was of the order of 2% (20 000 ppm).

The results given in the present paper show that the influence of profile variation on vibration properties depends on the combined effects of mass- and

stiffness-distributions that result from the dimensional variations. In certain simple cases, where the imperfection can be represented as a point mass [2] which does not affect stiffness, or a crack [8] which does not significantly affect mass, the positions of given modes can be predicted intuitively from considerations of maximum and minimum kinetic energy or strain energy. In the case of general profile variations, however, the effects are more subtle and are not necessarily easy to predict intuitively. This is because, for example, thickening the ring in some region leads to an increase in both the mass and the stiffness in that region. It is the integrated balance of the variations over the entire ring that determines the circumferential location of the modes and whether the frequencies of particular modes will increase or decrease. This point will be discussed in more detail, with specific examples, later in the paper.

The present paper is structured as follows. A brief review of the key analytical results as developed in reference [1] is given. Numerical results relating to a number of examples of increasing complexity are then presented, starting with profiles containing only a single harmonic variation. The effects of profile harmonic number, profile variation amplitude and the relative phasing between the inner and outer surfaces are considered. More complicated examples with multiple-harmonic profile variations are presented, including a regular polygon. Finally, a general discussion of the interpretation of the results is given and conclusions are drawn.

2. METHOD OF ANALYSIS

The method of analysis used to obtain the numerical results presented in this paper is fully described in references [1, 9]. For convenience and ease of reference when discussing the numerical results, the key steps are repeated below in summary form.

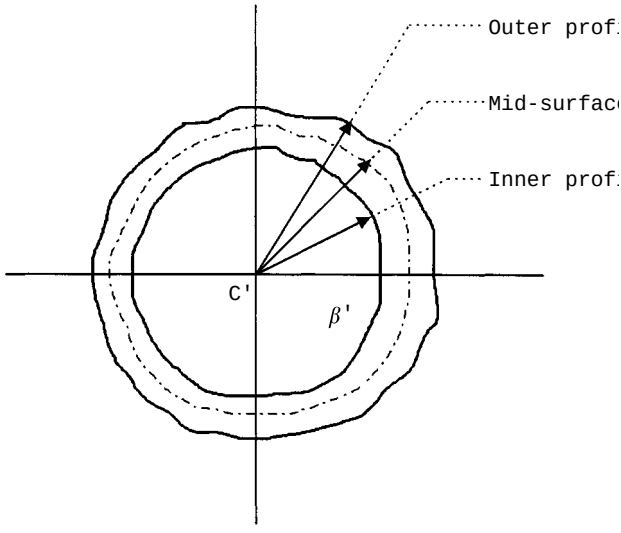

Figure 1. A thin ring having circumferentially arbitrary profile.

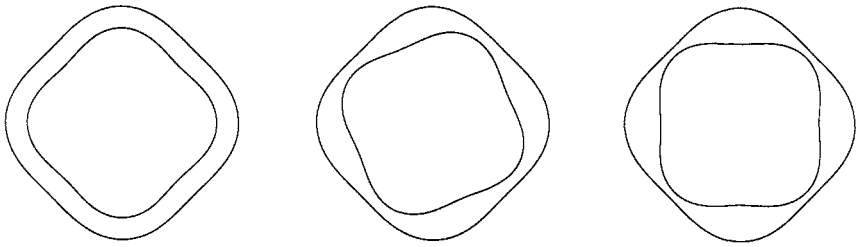

Figure 2. Illustration of spatial phase ($i = j = 4$; $h_f^+ = h_f^- = 0{\cdot}3h$).

Using Fourier series it is possible to model any closed ring bounded by single-valued curves (see Figure 1) as follows:

$$f^+(\beta') = f_0^+ + \sum_{p=1}^{n} f_p^+ \cos(p\beta') + \sum_{q=1}^{n} f_q^+ \sin(q\beta'), \tag{1}$$

$$f^-(\beta') = f_0^- + \sum_{p=1}^{n} f_p^- \cos(p\beta') + \sum_{q=1}^{n} f_q^- \sin(q\beta'), \tag{2}$$

where $f^+(\beta')$ and $f^-(\beta')$ denote respectively the outer and inner surface functions with respect to the global circumferential co-ordinate β' and $f_0^+, f_p^+, f_q^+, f_0^-, f_p^-$ and f_q^- are the Fourier coefficients.

One of the particular cases that will be considered here in some detail is that where the inner and outer surfaces are each assumed to contain only a single harmonic variation in profile. The harmonic number can be the same for both surfaces, or different. In these cases the outer and inner profile can be expressed quite generally as follows:

$$f^+(\beta') = r_a^+ + h_f^+ \cos i\beta', \qquad f^-(\beta') = r_a^- + h_f^- \cos(j\beta' - \phi), \tag{3, 4}$$

where h_f^+ and h_f^- are the amplitudes of the outer and inner surface profile variations measured from the mean outer and inner radii r_a^+ and r_a^-, respectively, and i, j are the harmonic numbers of the outer and inner profiles respectively.

ϕ may be referred to as the spatial phase angle between the trigonometric functions of the inner and outer surfaces at $\beta' = 0$. Figure 2 illustrates some examples of the case where the harmonic numbers of the inner and outer surfaces are the same ($=4$) but the spatial phase angles are different.

For free vibration at frequency ω the tangential and normal displacement, v and w, of the middle surface are assumed to have the following forms:

$$v = \sum_{n=0}^{N} (v_n^s \sin n\beta' - v_n^c \cos n\beta') \, e^{i\omega t}, \tag{5}$$

$$w = \sum_{n=0}^{N} (w_n^c \cos n\beta' + w_n^s \sin n\beta')\, e^{i\omega t}, \tag{6}$$

where v_n^c, v_n^s, w_n^c and w_n^s are the generalised co-ordinates.

Based on the above relationships, the eigenvalue problem for in-plane free vibration of the ring can be derived [9] using a suitable thin shell theory (e.g., Novozhilov's [10]) and the Rayleigh–Ritz method. It can be expressed in the following general matrix form

$$\left[\begin{bmatrix} \mathbf{K}^{ss} & \mathbf{K}^{sc} \\ \mathbf{K}^{cs} & \mathbf{K}^{cc} \end{bmatrix} - \lambda^2 \begin{bmatrix} \mathbf{M}^{ss} & \mathbf{M}^{sc} \\ \mathbf{M}^{cs} & \mathbf{M}^{cc} \end{bmatrix}\right] \begin{bmatrix} \mathbf{q}_s \\ \mathbf{q}_c \end{bmatrix} = \begin{bmatrix} \mathbf{0} \\ \mathbf{0} \end{bmatrix}, \tag{7}$$

where

$$\mathbf{q}_s = \begin{bmatrix} v_0^s \\ w_0^s \\ v_1^s \\ w_1^s \\ \vdots \\ \vdots \\ v_N^s \\ w_N^s \end{bmatrix}, \qquad \mathbf{q}_c = \begin{bmatrix} v_0^c \\ w_0^c \\ v_1^c \\ w_1^c \\ \vdots \\ \vdots \\ v_N^c \\ w_N^c \end{bmatrix}. \tag{8}$$

In the above equations, $\mathbf{q}$ denotes a vector of generalised co-ordinates v_n, w_n and $[\mathbf{K}^{ss}]$ etc. and $[\mathbf{M}^{ss}]$ etc. represent stiffness and mass matrices of size $2(N+1)$. The superscript s denotes coefficients related to co-ordinates v_n^s and w_n^s, and superscript c denotes coefficients related to co-ordinates v_n^c and w_n^c. The frequency factors of the ring, λ, are the eigenvalues of equation (7) and are defined by

$$\lambda_n = \sqrt{\frac{\rho}{E}}\, \omega_n r_a, \tag{9}$$

where ω_n is the natural frequency of the nth radial mode, r_a is the mean radius of the middle surface, E is Young's modulus and ρ is the density of the ring material.

The eigenvalue problem, equation (7), can be solved numerically, using one of the readily available standard techniques, to obtain the eigenvalues (the frequency factors) and the eigenvectors (the mode shapes). For a given value of n, equation (7) yields a pair of values of λ_n except at the $n = 0$ mode. The pair of eigenvalues will be equal in the case of a perfect ring but will be slightly different in the case of an imperfect ring, giving rise to a higher frequency mode and a lower frequency mode for each value of n.

3. NUMERICAL RESULTS

All the frequency data in this paper will be presented and discussed using the non-dimensional frequency factor λ_n defined by equation (9). In computing the results, sufficient terms have been used in the displacement solution series, equations (5) and (6), to achieve convergence to four significant figures in the frequency factors, this being a practical compromise between accuracy and computing time based on engineering judgement. The required convergence was met in most cases using 30 terms in the series and, unless otherwise stated, it may be assumed that 30 terms were used. The results presented are in very close agreement with those obtained from an extensive finite element study [9] giving confidence in their validity.

In presenting the numerical results, emphasis has been placed on the frequency-splitting effect of profile variations, since this was the initial motivation for performing the work and, in practice, frequency splitting is the most significant practical consequence of small departures from perfect circularity. In the main, therefore, absolute values of frequency factor are not quoted and the numerical frequency results are given as the percentage changes caused by profile variation compared to the perfect ring. Details of actual frequency factors, and of comparison with results derived from finite element analysis, may be found in reference [9].

Nominal ring dimensions and material properties used in this paper are the same as those adopted by Tonin and Bies [7], namely $r_a^+ = 40{\cdot}75$ mm, $r_a^- = 37{\cdot}83$ mm, $E = 206{\cdot}7 \times 10^9$ N/m^2, $\rho = 7850$ kg/m^3. The axial length is 2 mm.

3.1. SINGLE-HARMONIC PROFILE VARIATIONS

In general, it is unlikely that imperfections in the manufacturing process would lead to a ring which contained only a single harmonic departure from true circularity in both the inner and outer surfaces, although it is well known that the method of support of circular components (such as ball bearing raceways) during turning and grinding operations can induce lobed shapes which are dominated by a single harmonic. Nevertheless, a sound understanding of the individual effect of a single profile variation harmonic on the vibration of the ring would seem to be a logical precursor to an investigation of what happens when multiple profile variation harmonics are present. We therefore begin by examining in some detail the effect of a single harmonic component.

Clearly there is an almost infinite range of harmonic numbers (i, j) and profile harmonic amplitudes, h_f^+ and h_f^-, (equations (3) and (4)) which could be investigated. From practical considerations, results will be restricted mainly to cases where the inner and outer profiles contain harmonic numbers in the range $i = j = 1, 2, 3, 4, 5, 6$. Furthermore, it will be assumed that the profile harmonic amplitude is the same on the inner and outer surfaces and values of h_f within the range $h_f^+ = h_f^- = 0{\cdot}01h$ to $0{\cdot}6h$ will be considered, where $h = r_a^+ - r_a^-$ is the difference between the mean outer and inner radii. This range of profile amplitudes encompasses what might be termed both "small" and "large" variations. Spatial phases in the range $\phi = 0$ to π will be considered.

3.1.1. *The effect of profile harmonic number*

Tables 1 and 2 show the effect of a single harmonic profile variation with harmonic number in the range 1 to 6 for a profile amplitude $h_f^+ = h_f^- = 0{\cdot}1h$ and three values of the spatial phase angle ϕ. The results for even profile harmonics are given in Table 1 and for odd harmonics in Table 2. They are displayed separately because the frequency splitting patterns are different for the two cases. The results in the tables show the percentage differences between the frequency factors λ_n for the ring with profile variations present compared to the corresponding frequency factor of the equivalent perfect ring (i.e., ring with $h_f^+ = h_f^- = 0$). In the tables, percentage differences are displayed to two decimal places consistent with the four significant figure accuracy of the frequency factors. The column headings, $\omega(n)$, refer to the predominant harmonic number, n, in the corresponding eigenvector (mode shape vector). For example, $\omega(2)$ refers to a mode in which the dominant component of the eigenvector is the $2\beta'$ contribution. In the case of a perfect ring this eigenvector would contain *only* the $2\beta'$ contribution, but when the ring profile is no longer purely circular the corresponding eigenvector contains relatively small components at $3\beta'$, $4\beta'$, ... etc. This will be discussed in more detail later in the paper.

Where frequency splitting occurs in a particular doublet, two different values of percentage change in λ_n are shown in Tables 1 and 2 and these are identified in the third column as being the higher and lower frequencies in the pair. The

TABLE 1

The effect of even profile harmonic numbers on frequency factor

		Frequency	$\omega(0)$	$\omega(2)$	$\omega(3)$	$\omega(4)$	$\omega(5)$	$\omega(6)$
$\phi = 0$	$i = j = 2$	High	−0·01	**−0·01**	−0·02	−0·02	−0·02	−0·02
		Low		**−0·02**	−0·02	−0·02	−0·02	−0·02
	$i = j = 4$	High	0·23	**1·07**	−0·07	**−0·08**	−0·17	−0·12
		Low		**−1·15**	−0·07	**−0·30**	−0·17	−0·12
	$i = j = 6$	High	2·79	**−0·09**	**1·20**	−0·13	−0·36	**−0·15**
		Low		**−0·09**	**−1·37**	−0·13	−0·36	**−2·85**
$\phi = \pi/2$	$i = j = 2$	High	≈0	**0·17**	**−0·30**	−0·49	−0·59	−0·64
		Low		**−1·22**	**−0·34**	−0·49	−0·59	−0·64
	$i = j = 4$	High	0·19	**7·04**	**−0·58**	**0·14**	−0·44	**−0·42**
		Low		**−9·84**	−0·58	**−1·45**	−0·44	**−0·45**
	$i = j = 6$	High	2·04	−2·85	**6·36**	−0·66	−0·71	**−0·06**
		Low		−2·85	**−9·22**	−0·66	−0·71	**−3·24**
$\phi = \pi$	$i = j = 2$	High	0·01	**0·34**	**−0·57**	−0·96	−1·16	−1·27
		Low		**−2·44**	**−0·67**	−0·96	−1·16	−1·27
	$i = j = 4$	High	0·16	**9·00**	**−1·12**	**0·26**	−0·70	**−0·73**
		Low		**−14·53**	**−1·12**	**−2·53**	−0·70	**−0·77**
	$i = j = 6$	High	1·40	−5·56	**8·06**	−1·21	−1·07	**−0·95**
		Low		−5·56	**−13·61**	−1·21	−1·07	**−2·56**

$h_f^+ = h_f^- = 0{\cdot}1h$; $\omega(n)$ denotes mode dominated by nth displacement harmonic. Numerical values are percentage change in frequency factor λ_n compared to perfect ring, defined as $[\lambda_n^{imperfect} - \lambda_n^{perfect}] \times 100\%/\lambda_n^{perfect}$.

TABLE 2

The effect of odd profile harmonic numbers on frequency factor

		Frequency	$\omega(0)$	$\omega(2)$	$\omega(3)$	$\omega(4)$	$\omega(5)$	$\omega(6)$
$\phi = 0$	$i = j = 1$	High	≈ 0	≈ 0	≈ 0	≈ 0	≈ 0	≈ 0
		Low		≈ 0	≈ 0	≈ 0	≈ 0	≈ 0
	$i = j = 3$	High	0·04	−0·02	**−0·04**	−0·07	−0·05	−0·05
		Low		−0·02	**−0·08**	−0·07	−0·05	−0·05
	$i = j = 5$	High	0·81	−0·09	−0·07	−0·17	**−0·11**	−0·42
		Low		−0·09	−0·07	−0·17	**−0·91**	−0·42
$\phi = \pi/2$	$i = j = 1$	High	≈ 0	−0·29	−0·61	−0·69	−0·71	−0·72
		Low		−0·29	−0·61	−0·69	−0·71	−0·72
	$i = j = 3$	High	0·05	−0·62	**0·17**	−0·36	−0·44	−0·52
		Low		−0·62	**−1·29**	−0·36	−0·44	−0·52
	$i = j = 5$	High	0·62	−2·86	−0·62	−0·60	**0·11**	−0·59
		Low		−2·86	−0·62	−0·60	**−1·87**	−0·59
$\phi = \pi$	$i = j = 1$	High	≈ 0	**−0·57**	−1·23	−1·38	−1·43	−1·45
		Low		**−0·58**	−1·23	−1·38	−1·43	−1·45
	$i = j = 3$	High	0·05	−1·24	**0·35**	−0·66	−0·82	−1·00
		Low		−1·24	**−2·50**	−0·66	−0·82	−1·00
	$i = j = 5$	High	0·44	−5·60	−1·21	−1·07	**−0·01**	−0·76
		Low		−5·60	−1·21	−1·07	**−2·55**	−0·76

$h_f^+ = h_f^- = 0{\cdot}1h$; $\omega(n)$ denotes mode dominated by nth displacement harmonic. Numerical values are percentage change in frequency factor λ_n compared to perfect ring, defined as $[\lambda_n^{imperfect} - \lambda_n^{perfect}] \times 100\%/\lambda_n^{perfect}$.

frequency split in a given doublet is the arithmetic difference between the higher and lower values.

Turning now to a detailed examination of the results presented in Tables 1 and 2, the following observations may be made about the frequency splitting patterns of the flexural modes (there is no frequency splitting of the $\omega(0)$, breathing, mode).

(a) When the profile variation harmonic number ($i = j$) is *even* (Table 1), frequency splitting only occurs in the nth mode when $n = ki/2$ where k is a positive integer. (The split frequencies are highlighted in the table.) For example, it can be seen from Table 1 that for the case where $i = j = 4$, $\phi = 0$ that the frequency factor percentage splits are 2·22% for $n = 2$ (i.e., $\omega(2)$), 0·22% for $n = 4$ (i.e., $\omega(4)$) and less than 0·01% for $n = 6$. Frequency splitting continues to be predicted for higher values of n but is smaller than the 0·01% accuracy of the computed results. Similar trends can be seen for all even values of i and j. It may be noted that the maximum split for a given $i = j$ occurs at the lowest value of n and the split becomes smaller at higher values of n.

(b) When the profile variation harmonic number ($i = j$) is *odd* (Table 2), frequency splitting only occurs in the nth mode when $n = ki$ where k is a positive integer. For example, it can be seen from Table 2 that for the case where $i = j = 3$ and $\phi = 0$ that splitting of 0·04% occurs for $n = 3$ (i.e., $\omega(3)$). As in the case where n is even, the frequency split is largest for the lowest value of n and becomes smaller for higher values of n. In fact, for the profile amplitude $h_f^+ = h_f^- = 0{\cdot}1h$ on which Table 2 is based, the frequency split is less than 0·01% for $k > 1$, so the splits do

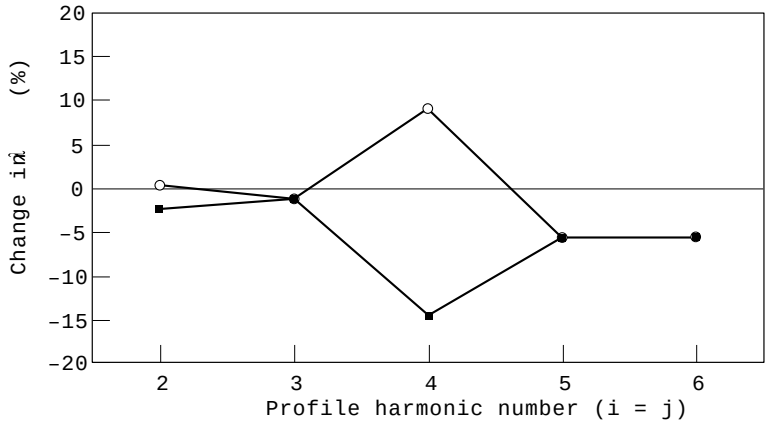

Figure 3. Effect of profile harmonic number ($i = j$) on frequency factors of 2nd mode ($n = 2$) ($\phi = \pi$, $h_f = 0{\cdot}1h$). —○—, Higher frequency; —■—, lower frequency.

not show in the tabulated values. Larger values of h_f^+ and h_f^- will be considered later.

It is noticeable that, for the same amplitude of profile variation harmonic, the frequency splits which occur when the profile harmonics are even and $n = i/2$ are generally much greater than those which occur when $n = i$ for i even or odd. Possible reasons for this will be discussed in section 4 of the paper.

Figures 3–5 illustrate the principal trends relating to the effects of harmonic number which follow from Tables 1 and 2. It is noteworthy that the trends in frequency splitting resulting from single harmonic components of profile variation are in agreement with the splitting rules established in reference [4] for the case of equal attached masses placed at the vertices of regular polygons with the same harmonic number.

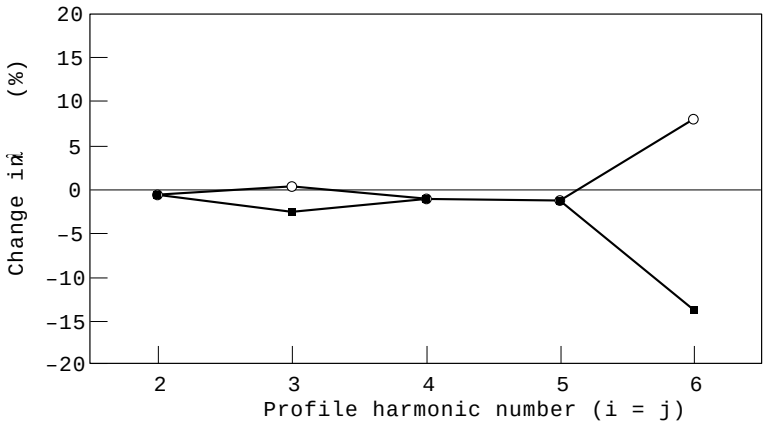

Figure 4. Effect of profile harmonic number ($i = j$) on frequency factors of 3rd mode ($n = 3$) ($\phi = \pi$, $h_f = 0{\cdot}1h$). —○—, Higher frequency; —■—, lower frequency.

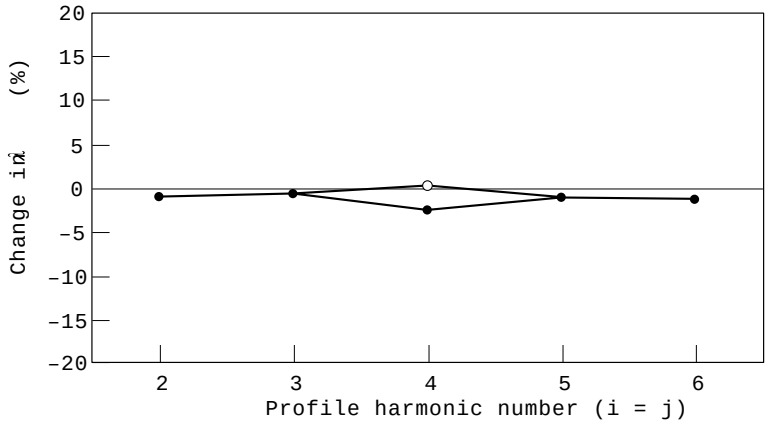

Figure 5. Effect of profile harmonic number ($i = j$) on frequency factors of 4th mode ($n = 4$) ($\phi = \pi$, $h_f = 0{\cdot}1h$). —○—, Higher frequency; —■—, lower frequency.

3.1.2. *The effect of spatial phase angle*

The spatial phasing between the single harmonic profile variation on the outer and inner surfaces has a strong influence on frequency splitting. In general it is found that frequency splitting increases significantly when the spatial phase angle

TABLE 3

Modal vectors of the 2nd and 3rd modes ($i = j = 2$, $\phi = 0$, *and* $h_f^+ = h_f^- = 0{\cdot}1h$)

Frequency factors		Contribution to modal vector from nth generalised co-ordinate						
λ_n	$n =$	0	1	2	3	4	5	6
0·0576	w_n^c	−0·0133	0·00	0·8943	0·00	0·0057	0·00	0·00
	w_n^s	0·00	0·00	0·00	0·00	0·00	0·00	0·00
2nd mode	v_n^s	0·00	0·00	−0·4473	0·00	−0·0047	0·00	0·00
	v_n^c	0·00	0·00	0·00	0·00	0·00	0·00	0·00
0·0575	w_n^c	0·00	0·00	0·00	0·00	0·00	0·00	0·00
	w_n^s	0·00	0·00	0·8942	0·00	0·0057	0·00	0·00
2nd mode	v_n^s	0·00	0·00	0·00	0·00	0·00	0·00	0·00
	v_n^c	0·0100	0·00	−0·4475	0·00	−0·0047	0·00	0·00
0·1626	w_n^c	0·00	−0·0140	0·00	0·9483	0·00	0·070	0·00
	w_n^s	0·00	0·00	0·00	0·00	0·00	0·00	0·00
3rd mode	v_n^s	0·00	0·0001	0·00	−0·3170	0·00	−0·0042	0·00
	v_n^c	0·00	0·00	0·00	0·00	0·00	0·00	0·00
0·1626	w_n^c	0·00	0·00	0·00	0·00	0·00	0·00	0·00
	w_n^s	0·00	−0·0143	0·00	0·9483	0·00	0·070	0·00
3rd mode	v_n^s	0·00	0·00	0·00	0·00	0·00	0·00	0·00
	v_n^c	0·00	−0·0003	0·00	−0·3170	0·00	−0·0042	0·00

Note, only even n contributors are $\neq 0$ in the 2nd mode and only odd n contributors are $\neq 0$ in the 3rd mode. Frequency split $\equiv 0$ in the 3rd mode. Modal vectors are normalised such that RSS of all components = 1 (30-term series).

TABLE 4

Modal vectors of the 2nd and 3rd modes ($i = j = 4$, $\phi = \pi$, *and* $h_f^+ = h_f^- = 0{\cdot}1h$)

Frequency factors		Contribution to modal vector from nth generalised co-ordinate						
λ_n	$n =$	0	1	2	3	4	5	6
0·0627	w_n^c	0·00	0·00	0·8940	0·00	0·00	0·00	−0·0250
	w_n^s	0·00	0·00	0·00	0·00	0·00	0·00	0·00
2nd mode	v_n^s	0·00	0·00	−0·4474	0·00	0·00	0·00	0·0042
	v_n^c	0·00	0·00	0·00	0·00	0·00	0·00	0·00
0·0492	w_n^c	0·00	0·00	0·00	0·00	0·00	0·00	0·00
	w_n^s	0·00	0·00	0·8941	0·00	0·00	0·00	−0·0206
2nd mode	v_n^s	0·00	0·00	0·00	0·00	0·00	0·00	0·00
	v_n^c	0·00	0·00	−0·4474	0·00	0·00	0·00	0·0034
0·1608	w_n^c	0·00	−0·0300	0·00	0·9464	0·00	−0·0111	0·00
	w_n^s	0·00	0·00	0·00	0·00	0·00	0·00	0·00
3rd mode	v_n^s	0·00	0·0320	0·00	−0·3164	0·00	0·0022	0·00
	v_n^c	0·00	0·00	0·00	0·00	0·00	0·00	0·00
0·1608	w_n^c	0·00	0·00	0·00	0·00	0·00	0·00	0·00
	w_n^s	0·00	−0·0300	0·00	−0·9464	0·00	−0·0111	0·00
3rd mode	v_n^s	0·00	0·00	0·00	0·00	0·00	0·00	0·00
	v_n^c	0·00	−0·0320	0·00	0·3164	0·00	0·0022	0·00

Note, only even n contributors are $\neq 0$ in the 2nd mode and only odd n contributors are $\neq 0$ in the 3rd mode. Frequency split $\equiv 0$ in the 3rd mode. Modal vectors are normalised such that RSS of all components = 1 (30-term series).

increases from 0 to π. Before examining the numerical results in detail it is worth commenting on the physical meaning of spatial phase. Consider Figure 2 which shows schematically (profile variation amplitude is exaggerated for clarity) a ring with equal amplitude $4\beta'$ variations in the inner and outer profiles for three values of spatial phase ϕ ($=0, \pi/2, \pi$). $\phi = 0$ and π are special cases of the more general case which is represented by $\pi/2$. In the case where $\phi = \pi$, Figure 2(c), the circumferential mid-surface is circular and the thickness has a $4\beta'$ harmonic variation. It can be seen that the difference between the maximum and minimum radial thickness is greatest in the case where $\phi = \pi$. At the other extreme, when $\phi = 0$, Figure 2(a), the mid-surface is non-circular and simply follows the mean of the inner and outer profiles. The corresponding thickness measured along the normal to the mid-surface is constant in this case. In both the above mentioned special cases the eigenvalue problem, equation (7), partitions into two uncoupled problems because the off-diagonal sub-matrices of the mass and stiffness matrices are zero. The resulting mode shapes are either symmetric or anti-symmetric with respect to $\beta' = 0$. Tables 3 and 4 show typical modal vectors which display these properties. For values of ϕ other than 0 and π the eigenvalue problem does not partition and the corresponding eigenvectors therefore contain a combination of odd and even (sine and cosine) generalised co-ordinates.

Returning now to the numerical frequency results it can be seen from Tables 1 and 2 that frequency splitting generally increases significantly when the spatial

phase angle increases from 0 to π. This is particularly marked in the splits which occur in modes for which $n = i/2$ when the profile harmonic number is even. For example, in Table 1 the frequency split in the $3\beta'$, $\omega(3)$, modes caused by a $6\beta'$ variation in profile ($i = j = 6$) is 2·57% when $\phi = 0$, 15·58% when $\phi = \pi/2$ and 21·67% when $\phi = \pi$. Similar figures apply to the split in the $2\beta'$ modes caused by a fourth harmonic profile variation, $i = j = 4$.

In the general case, there is no obvious, simply physical link between the geometry of the ring and the frequency splitting behaviour. However, in the special case i, j even, $\phi = \pi$, it may be possible to place a physical interpretation on the very large splitting which occurs in the $n = i/2$ modes. To aid this explanation, refer to Table 4 which shows the contribution to the modal vectors from the generalised co-ordinates corresponding to $n = 0, 1, 2, \ldots, 6$ for the case where $i = j = 4$ and $\phi = \pi$. This corresponds to the ring shape shown in Figure 2(c) where the profile varies as $\cos 4\beta'$. Table 1 indicates that a large (23·53%) frequency split occurs in the $2\beta'$ modes for this ring for $\phi = \pi$. The modal vectors corresponding to these modes are shown in Table 4 from which it can be seen that the radial (w) displacement pattern in the higher frequency mode is dominated by a $\cos 2\beta'$ distribution while the lower frequency mode is dominated by a $\sin 2\beta'$ distribution. This means that the maximum change in centreline curvature in the higher frequency mode occurs where the ring is thickest and therefore stiffest. Conversely, the maximum change in curvature in the lower frequency mode occurs where the ring is thinnest and therefore weakest. This ties in logically with the pattern of frequency splitting. Of course, it is also true that, in the higher frequency mode, the points of maximum displacement are points of maximum mass per unit length (and vice versa) which, taken by itself, would lead to the opposite pattern of frequency splitting (i.e., added mass at points of maximum displacement tends to lower the natural frequency). However, because the mass per unit length is directly proportional to the radial thickness but the flexural rigidity is proportional to the cube of the radial thickness, the "stiffness" effect dominates the "mass" effect, as it does in uniform beams where flexural natural frequencies increase with thickness.

It is more difficult to place a simple physical interpretation on more general cases where the ring geometry variation is less distinct, and there is possibly little practical value in pursuing this line any further at this stage. Suffice to say that the behaviour will be governed by the detailed structure of the mass and stiffness matrices which are derived from the strain energy and kinetic energy expressions which are given in reference [1]. These will be discussed in more detail in section 4 of the present paper.

The key general points about the way in which the profile harmonic number and spatial phase affect the frequency splitting are summarised in Figure 6 which shows the effects on the $2\beta'$ flexural modes of $2\beta'$, $3\beta'$ and $4\beta'$ variations in profile for spatial phases in the range 0 to π. The very large frequency splits caused by the $4\beta'$ profile variation are clearly demonstrated, as is the lack of any splitting at all due to the $3\beta'$ profile variation.

It may also be noted from Tables 1 and 2 that, irrespective of whether frequency splitting occurs, the effect of imperfection is generally to lower the natural frequencies of the flexural modes of the ring compared to the equivalent perfect

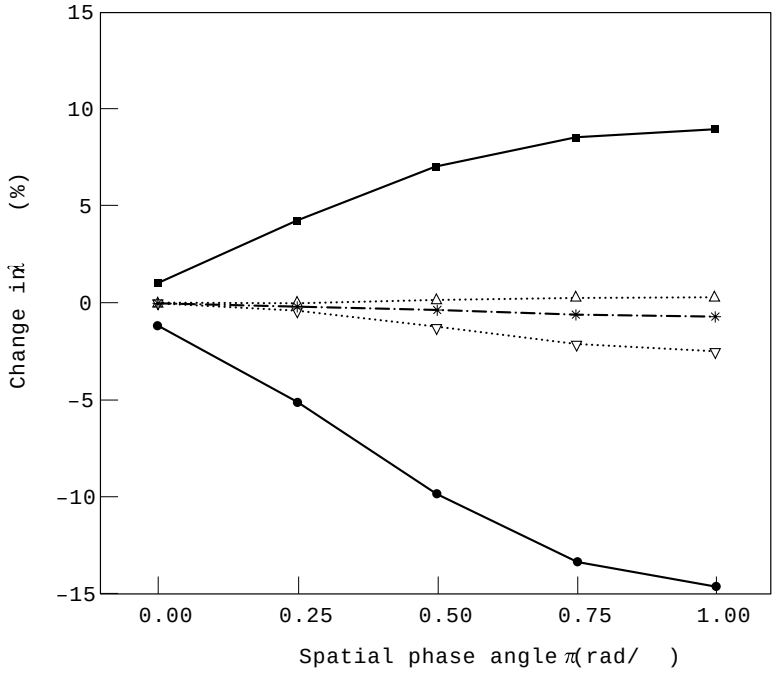

Figure 6. Effect of spatial phase angle on frequency factors of 2nd mode ($h_f = 0{\cdot}1h$]. —■—, High, $i = j = 4$; —●—, low, $i = j = 4$; . . . △ . . . , high, $i = j = 2$; . . . ▽ . . . , low, $i = j = 2$; —+—, High, $i = j = 3$; –.×–. , low, $i = j = 3$.

ring (i.e., most of the percentage changes in frequency factor are negative). The exceptions to this rule are the higher frequency modes in those doublets where significant frequency splitting occurs. It may be surmised that the general reduction in frequencies is linked with the fact that any imperfection tends to increase the length of the mid-surface, which would tend to lower the natural frequency.

3.1.3. *The effect of profile amplitude*

It is clear that the amplitude of the profile variation will have an important influence on the magnitude of the resulting frequency splits. In practice, the amplitude of any profile variation due to deficiencies in manufacturing processes are likely to be a small fraction of the mean radial thickness of the ring, and we will consider examples relevant to this case. However, it is also of interest to consider a range of larger profile variations where the profile amplitude is a significant fraction of the mean radial thickness. These are relevant, partly for the sake of completeness and partly because such cases provide a simple first order approximation to thin regular polygonal rings which will be considered in more detail later in the paper.

Consider first an example of a "small" profile variation. Table 5 compares the percentage changes in the frequency factors for the case where $i = j = 4$ for profile amplitudes of $0{\cdot}1h$ and $0{\cdot}01h$, respectively. It is immediately obvious that reducing the profile amplitude from $0{\cdot}1h$ to $0{\cdot}01h$ significantly reduces the frequency splitting to the extent that, to within the accuracy of the computed results, some

TABLE 5

Effect of profile amplitude on frequency factor

	h_f^+	Frequency	$w(0)$	$w(2)$	$w(3)$	$w(4)$	$w(5)$	$w(6)$
$\phi = 0$	$0{\cdot}1h$	High	0·23	1·07	−0·07	−0·08	−0·17	−0·12
		Low		−1·15	−0·07	−0·30	−0·17	−0·12
	$0{\cdot}01h$	High	≈0	0·11	≈0	≈0	≈0	≈0
		Low		−0·11	≈0	≈0	≈0	≈0
$\phi = \pi/2$	$0{\cdot}1h$	High	0·19	7·04	−0·58	0·14	−0·44	−0·42
		Low		−9·84	−0·58	−1·45	−0·44	−0·45
	$0{\cdot}01h$	High	≈0	0·84	−0·01	≈0	≈0	≈0
		Low		−0·87	−0·01	−0·01	≈0	≈0
$\phi = \pi$	$0{\cdot}1h$	High	0·16	9·00	−1·12	0·26	−0·70	−0·73
		Low		−14·53	−1·12	−2·53	−0·70	−0·77
	$0{\cdot}01h$	High	≈0	1·17	−0·01	≈0	−0·01	−0·01
		Low		−1·23	−0·01	−0·03	−0·01	−0·01

$h_f = 0{\cdot}01h$ and $0{\cdot}1h$; $\phi = 0$, $\pi/2$ and π; $i = j = 4$. $\omega(n)$ denotes mode dominated by nth displacement harmonic. Numerical values are percentage change in frequency factor λ_n compared to perfect ring, defined as $[\lambda_n^{imperfect} - \lambda_n^{perfect}] \times 100\%/\lambda_n^{perfect}$.

of the frequency splits disappear. Amongst those splits that remain, it may be noted that the relationship between magnitude of frequency split and amplitude of profile variation is different for those cases where $n = i/2$ compared to the cases where $n \neq i/2$. In the former case, reduction in the profile amplitude by a factor of 10 produces an approximately tenfold reduction in the frequency split (e.g., 23·53% to 2·4% for $\phi = \pi$ in the $n = 2$ modes). In the latter cases, however, the tenfold reduction in profile amplitude reduces the frequency split by a factor of the order of 100 (e.g., 2·79% to 0·03% for $\phi = \pi$ in the $n = 4$ modes). An almost identical pattern is observed for the corresponding frequency splits when $i = j = 6$ [9]. In cases where the profile variation harmonic is odd ($i = j = 3, 5, \ldots$), there are no modes corresponding to $n = i/2$ and it is found that the reduction in frequency split for the modes for which $n = i$ is of the order of 100 for a tenfold reduction in profile amplitude, as it is in the corresponding cases when i and j are even. Further detailed numerical results are available in reference [9].

In practical terms therefore there is a poweful incentive to reduce the magnitude of the profile variation if frequency splitting is to be minimised. The frequency split in a pair of modes, due to profile variations at twice the predominant mode-shape harmonic, is likely to be the most difficult to deal with practically. This is because such frequency splits are relatively much larger and the relationship between the profile-amplitude and the frequency split is apparently less strong (i.e., linear instead of quadratic). A detailed explanation of the differences in the profile amplitude and frequency split requires a more detailed consideration of the construction of the mass and stiffness matrices, which is given in section 4.

Consider now the situation where the profile amplitude is relatively large compared to the mean radial thickness. As an example, results are presented for

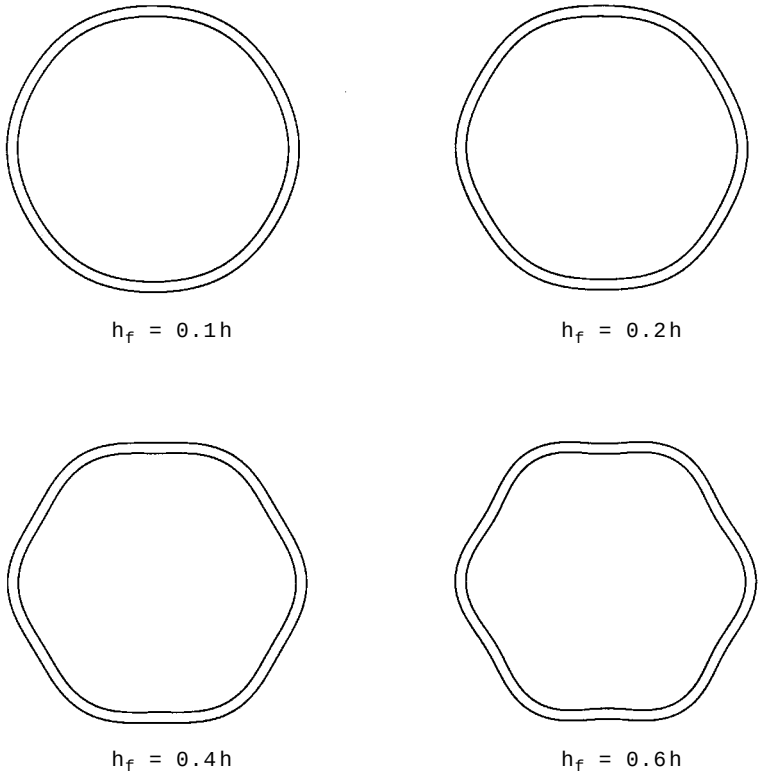

Figure 7. Geometry of ring with different amplitudes of 6th harmonic profile variation ($\phi = 0$).

a sixth harmonic variation in profile amplitude, such that the outer and inner profiles are given by

$$f^+(\beta') = r_a^+ + h_f \cos 6\beta', \qquad f^-(\beta') = r_a^- + h_f \cos (6\beta' - \phi), \qquad (10, 11)$$

where r_a^+ and r_a^- denote the nominal radii of outer and inner profiles, respectively, and $\phi = 0$.

Figure 7 illustrates the geometries considered and it can be seen that the resulting ring approximates to a hexagon for larger values of h_f. As an aside it may be noted here that when h_f^+ and h_f^- are greater than $h/2$, values of ϕ other than $\phi = 0$ could result in physically unrealisable rings in which the "inner" and "outer" profiles cross.

For the cases considered it was found that, within the accuracy of the computed results, frequency splitting is only predicted in the $3\beta'$ and $6\beta'$ modes and no splitting is predicted in the $2\beta'$, $4\beta'$ and $5\beta'$ modes. The percentage frequency splits in the $3\beta'$ and $6\beta'$ modes are, for the range of h_f considered, shown in Figure 8. As expected, the magnitidue of the frequency split increases as the profile amplitude increases. However, in contrast to the "small" amplitude profile variations considered earlier, the frequency split in the $6\beta'$ mode due to the $6\beta'$ profile variation is greater than the split in the $3\beta'$ mode for values of h_f greater than $\sim 0{\cdot}1$h. Extrapolation of the frequency split in the $3\beta'$ mode shown in

Figure 8 to include values of h_f in the range $0 < h_f < 0.1h$ indicates an almost linear relationship between profile amplitude and frequency split, as observed and discussed earlier in relation to the "small" amplitude profile variations. However, the almost-quadatic relationship between the profile amplitude and frequency split in the $6\beta'$ modes which was demonstrated for $0{\cdot}01 < h_f < 0{\cdot}1h$ is not followed for $h_f > 0{\cdot}1h$ where the relationship appears to be almost linear in the range of h_f considered.

3.2. MULTI-HARMONIC PROFILE VARIATIONS

It is most unlikely that the profile variation on the inner and outer surfaces of a real ring would contain only a single harmonic. The more general case where a significant number of harmonics of different amplitude exists on the inner and outer surfaces is not particularly tractable. In order to progress from the single harmonic variation considered in section 3.1 towards the general case, results are now presented for three cases of intermediate complexity, each of which contains a small number of different harmonics. These cases are: (i) the inner and outer profile each contain a single, (different) harmonic, (ii) the inner and outer profiles each contain the same three harmonics, and (iii) a regular hexagonal ring.

3.2.1. *Different single harmonic on inner and outer profile*

Table 6 shows the changes in frequency factors compared to those of a perfect ring, for a number of cases, these being $i = j = 3, 4, 6$ together with the combinations $i = 3$, $j = 4$ and $i = 4$, $j = 6$, with $\phi = \pi$ and $h_f^+ = h_f^- = 0{\cdot}1h$ in all cases.

The patterns of frequency splitting in the cases where only a single harmonic is present are of course the same as those discussed in section 3.1 and the frequency splits are maxima because $\phi = \pi$. In the cases where two different harmonics are present, frequency splits occur in those modes which would be expected from each of the single harmonic contributions taken separately, albeit that the predicted

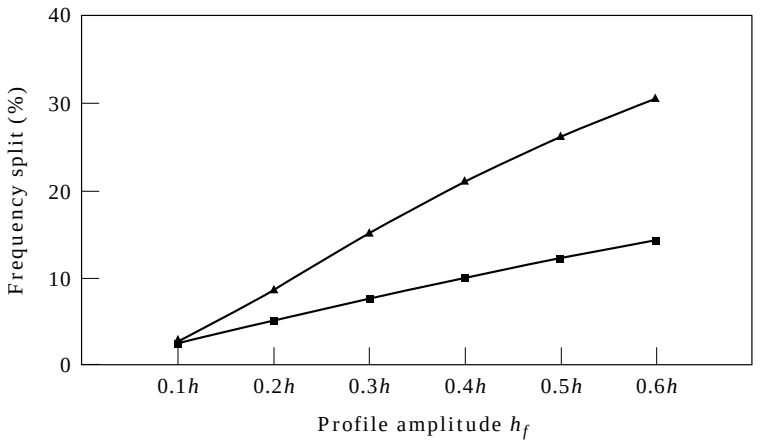

Figure 8. The frequency split versus profile amplitude varied from $0{\cdot}1h$ to $0{\cdot}6h$ in the 3rd and 6th modes. —■—, 3rd mode; —▲—, 6th mode.

TABLE 6

Effect of combinations of two profile harmonics on frequency factors ($h_f = 0{\cdot}1h$, $\phi = \pi$)

	Frequency	$w(0)$	$w(2)$	$w(3)$	$w(4)$	$w(5)$	$w(6)$
$i = j = 3$	High	0·05	−1·24	0·35	−0·66	−0·82	−1·00
	Low		−1·24	−2·50	−0·66	−0·82	−1·00
$i = j = 4$	High	0·16	9·00	−1·12	0·26	−0·70	−0·73
	Low		−14·53	−1·12	−2·53	−0·70	−0·77
$i = j = 6$	High	1·40	−5·56	8·06	−1·21	−1·07	−0·95
	Low		−5·56	−13·61	−1·21	−1·07	−2·56
$i = 3, j = 4$	High	0·18	5·37	−0·14	−0·44	−0·50	−0·49
	Low		−7·39	−0·96	−0·82	−0·51	−0·51
$i = 4, j = 6$	High	2·15	3·30	5·02	−0·17	0·26	−0·91
	Low		−7·71	−6·98	−0·90	−1·57	−2·42

$\omega(n)$ denotes mode dominated by nth displacement harmonic. Numerical values are percentage change in frequency factor λ_n compared to perfect ring, defined as $[\lambda_n^{imperfect} - \lambda_n^{perfect}] \times 100\%/\lambda_n^{perfect}$.

frequency splits are proportionally smaller due to the reduced level of profile variation at each value of i and j. Additionally, however, a frequency split is predicted in the $\omega(5)$ modes which is not caused by either of the two harmonics individually. The actual level of this frequency split in the case $i = 4$, $j = 6$ is significant (1·83%), but is much smaller (0·01%) in the case $i = 3, j = 4$. The cause of this "cross splitting" will be discussed in section 4.

3.2.2. *Three harmonics on the outer and inner surfaces*

To move towards the general case, consider outer and inner profiles defined by the following three-term series

$$f^+(\beta') = r_a^+ + 0{\cdot}01h \cos 3\beta' + 0{\cdot}05h \cos 4\beta' + 0{\cdot}1h \cos 6\beta', \tag{12}$$

$$f^-(\beta') = r_a^- + 0{\cdot}01h \cos (3\beta' - 0) + 0{\cdot}05h \cos (4\beta' - \pi/2) + 0{\cdot}1h \cos (6\beta' - \pi), \tag{13}$$

where r_a^+ and r_a^- denote the mean radii of outer and inner profiles, respectively, and h is the mean thickness of the ring.

Table 7 presents the percentage frequency splits for each of the three harmonic profile variations taken individually and in combination. As before, the pattern of frequency splitting due to each harmonic taken individually is as expected. It can be seen that in the single harmonic cases, particularly large splits (21·65% in the $\omega(3)$ mode for $i = j = 6$ and 8·5% in the $\omega(2)$ modes for $i = j = 4$) are predicted.

When all the profile variation harmonics are taken together, it can again be seen that frequency splits occur at all the frequencies where splits occur due to single harmonics. In addition, a frequency split is predicted in the $\omega(5)$ modes due to the combined effect of the harmonics. However, it is particularly striking that the previously large magnitudes of the splits in the $\omega(2)$ and $\omega(3)$ modes are much reduced (8·5%→1·09% and 21·65%→2·58%) in the combined case, even though

TABLE 7

Effect of combinations of three profile harmonics on frequency factors ($h_f = 0{\cdot}1h$, various ϕ)

Profile variations	Frequency split (%)				
	$\omega(2)$	$\omega(3)$	$\omega(4)$	$\omega(5)$	$\omega(6)$
$h_f = 0{\cdot}01h$ $i = j = 3$, $\phi = 0$	≈ 0	≈ 0	≈ 0	≈ 0	≈ 0
$h_f = 0{\cdot}05h$ $i = j = 4$, $\phi = \pi/2$	8·50	≈ 0	0·39	≈ 0	≈ 0
$h_f = 0{\cdot}1h$ $i = j = 6$, $\phi = \pi$	≈ 0	21·65	≈ 0	≈ 0	1·62
Combination of above profile variations	1·09	2·58	0·06	0·28	2·68

$\omega(n)$ denotes mode dominated by nth displacement harmonic. Numerical values are percentage change in frequency factor λ_n compared to perfect ring, defined as $[\lambda_n^{imperfect} - \lambda_n^{perfect}] \times 100\%/\lambda_n^{perfect}$.

the profile harmonic amplitudes are the same in both cases. This can be rationalised on the grounds that a single harmonic variation in the inner and outer profiles, particularly when $\phi = \pi$, represents the most extreme variation of mass and stiffness distribution compared to the perfect ring. When multiple harmonics are present, however, the overall variation is diluted.

3.2.3. *Thin-walled regular polygons*

As the final example, consider a thin-walled polygon, typified by a hexagon. Any regular polygon can be described by a Fourier series which, for an n-sided polygon, contains only non-zero spatial harmonics of order kn where $k = 0, 1, 2, 3, \ldots$. Table 8 shows the Fourier coefficients for the thin-walled hexagonal ring considered here, from which it can be seen that the magnitude of the non-zero coefficients reduces steadily as k increases. In broad terms, the ratios of the 6th, 12th and 18th harmonic amplitudes to the mean thickness are of the

TABLE 8

Fourier coefficients of the hexagon

Outer profile	Inner profile
$a_0^+ = 0{\cdot}10881\text{e} + 01$	$a_0^- = 0{\cdot}10101\text{e} + 01$
$a_6^+ = -0{\cdot}63279\text{e} - 01$	$a_6^- = -0{\cdot}58745\text{e} - 01$
$a_{12}^+ = 0{\cdot}17545\text{e} - 01$	$a_{12}^- = 0{\cdot}16288\text{e} - 01$
$a_{18}^+ = -0{\cdot}79850\text{e} - 02$	$a_{18}^- = -0{\cdot}74128\text{e} - 02$
....	
and	
$a_{6n+1}^+ = a_{6n+2}^+ = a_{6n+3}^+ = a_{6n+4}^+ = a_{6n+5}^+ = 0,$	
$a_{6n+1}^- = a_{6n+2}^- = a_{6n+3}^- = a_{6n+4}^- = a_{6n+5}^- = 0,$	
and $b_n^+ = b_n^- = 0$ where $n = 0, 1, 2, 3, \ldots,$	

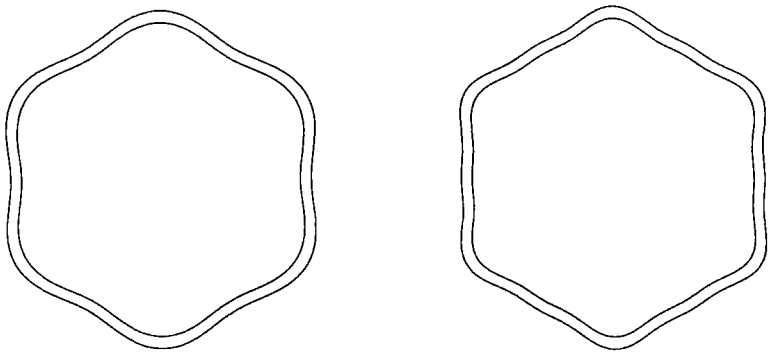

Figure 9. Hexagon geometry approximated by truncated Fourier series with p terms.

order 0·78, 0·22 and 0·1, respectively. Figure 9 shows the physical geometry of a hexagon approximated by 6-term and 12-term series (i.e., a circle plus one and two additional terms only).

Table 9 presents the percentage frequency splits predicted for 6-term ($p = 6$) and 12-term ($p = 12$) profile series for cases where $N = 30$ and $N = 40$ terms were used in the displacement function series, equations (5) and (6). In the case of the 12-term profile series it was found that $N = 30$ did not produce the required four significant figure convergence in the frequency factors, hence $N = 40$ was used. It can be seen from Table 9 that use of a 12-term profile series ($p = 12$) produces relatively small changes in the predicted frequency factors compared to the 6-term series ($p = 6$) and the magnitudes of the predicted splits in both cases are comparable with what would be predicted if the curves in Figure 8 were extrapolated to a profile amplitude in the region of $0{\cdot}78h$. Table 9 also includes the corresponding results from a Finite Element analysis of an "exact" hexagon [9]. The predicted splits are of the same order as those obtained using the numerical method. However, the level of discrepancy between the two methods suggests that more terms are needed in the profile series ($p = 18$, 24, etc.) to obtain an accurate representation of the

TABLE 9

Predicted frequency splitting of hexagon. Effect of number of terms used in profile Fourier series

p, N	$\omega(2)$	$\omega(3)$	$\omega(4)$	$\omega(5)$	$\omega(6)$
6, 30	≈ 0	11·4%	≈ 0	≈ 0	33·9%
12, 30	≈ 0	15·9%	≈ 0	≈ 0	35·1%
12, 40	≈ 0	17·0%	≈ 0	≈ 0	35·1%
12, FE	≈ 0	16·9%	≈ 0	≈ 0	40·5%
Exact			≈ 0		
Shape (FE)	≈ 0	15·2%		≈ 0	44·6%

p = number of terms in profile Fourier series; N = number of terms in displacement function series.

sharp corners of the hexagon, but this would significantly increase the computing time.

4. DISCUSSION

The numerical results presented in Section 3 demonstrate a variety of frequency splitting behaviour, the precise detail of which changes quite markedly as the detailed spatial-harmonic content of the ring profile changes, even when the profile only contains one or two harmonics. As mentioned earlier, the way in which particular profile variation harmonics influence particular modes of vibration will be determined by the way in which they affect the relevant elements of the mass and stiffness matrices in equation (7) which, in turn, govern the coupling between the generalised co-ordinates. Although, in the most general case, a specific and detailed interpretation is likely to be prohibitively complex, it is possible to gain some general insight into the problem by examining the strain energy and kinetic energy integrals from which the stiffness and mass matrices are formed.

The relevant integrals are fully defined in reference [1], equations (18) and (23). It is unnecessary to repeat the equations fully here and it is sufficient to note that both the kinetic energy and strain energy are expressed by integrals around the ring circumference which have the following general form,

$$E = \int_0^{2\pi} \{F[w^2(n\beta)]G[h(i\beta) + \alpha h^3(i\beta)]\}\, \mathrm{d}\beta. \tag{12}$$

Considering the integrand in equation (12) it should be noted that $F[w^2(n\beta)]$ is a function only of the ring displacements and their derivatives with respect to β and to time, and $G[h(i\beta) + \alpha h^3(i\beta)]$ is a function only of the ring profile geometry. By examining the conditions under which the integral in equation (12) might lead to a non-zero result, it is possible to infer something useful about how particular orders of profile harmonic interact with the particular generalised co-ordinates and hence affect particular modes of vibration. The *precise* detail of each specific case is however embedded in the integrals which are given in references [1, 9]. To see the general pattern it is first necessary to look in more detail at the forms of the functions F and G.

$F[w^2(n\beta)]$ is a quadratic function of the displacement functions associated with the series of generalised co-ordinates, given by equations (5) and (6) of the present paper. It is easy to show that any pair of harmonics, say n and m, in the assumed displacement series will give rise to terms within $F[w^2(n\beta)]$ which contain sines and cosines of $2n\beta$, $2m\beta$, $(n + m)\beta$ and $(n - m)\beta$.

The function $G[h(i\beta) + \alpha h^3(i\beta)]$ depends on the ring's radial thickness and on the cube of the thickness. For a thin ring, the parameter α may be taken to be small, reflecting the fact that terms associated with h^3 will generally be much smaller than terms associated with h. The general form of $G[h(i\beta) + \alpha h^3(i\beta)]$ will be determined by the form of the inner and outer profiles as expressed by equations (1) and (2). If the ring profile contains only a single harmonic variation, say i, then the function G will contain terms which are the sines and cosines of $i\beta$

(associated with both h and αh^3) and $3i\beta$ (associated with αh^3 only). If the ring profile contains two harmonics, say i and j, then the function G may contain terms which are the sines and cosines of $i\beta$, $j\beta$ (associated with both h and αh^3) and of $3i\beta$, $3j\beta$, $(2i + j)\beta$, $(2j + i)\beta$ and $(2j - i)\beta$ (associated with αh^3 only). If more than two harmonics are present in the ring profile, additional combinations of harmonics will appear in G. For example, with three profile harmonics i, j, k, there will be additional combinations of the form $(i + j \pm k)$ and $(i - j \pm k)$. Further elaboration of this point is unnecessary, other than to note that terms associated with h, as opposed to αh^3, will have the dominant influence because of their relative magnitude.

Bearing in mind that F and G contain sine and cosine functions of various combinations of harmonics then, based on the orthogonality properties of harmonic functions of different orders, it is now possible to determine the conditions under which equation (12) can lead to a non-zero result by looking for appropriate combinations of displacement and profile variation harmonics in the functions F and G, respectively. It is clear that equation (12) can only give a non-zero result when a particular net combination of harmonics in function F is matched by the same net combination of harmonics in function G.

The simplest case to consider is that in which the profile contains only a single harmonic, say i, in which case G will contain components at $i\beta$ (associated with both h and h^3) and $3i\beta$ (associated with αh^3 only). Considering two displacement harmonics, m and n, F will contain components at $2n\beta$, $2m\beta$, $(n + m)\beta$ and $(n - m)\beta$. Non-zero integrals may therefore result if either i or $3i$ is equal to either $2n$ or $2m$ or $(n + m)$ or $(n - m)$. Bearing in mind that the numerical results were obtained using displacement series containing 30 terms (i.e., $n, m = 0, \ldots, 30$) it is clear that, even in this simplest of cases, many combinations of m and n could potentially give rise to non-zero contributions to the energy integrals, hence giving rise to many potentially non-zero terms in the mass and stiffness matrices. Some of these terms will be more significant than others.

It may be argued that the most important terms in the mass and stiffness matrices are those which are closest to the leading diagonal. (In the case of a perfectly circular ring, the choice of generalised co-ordinates used here leads to mass and stiffness matrices which are diagonal.) This is consistent with the observation that, for rings with profile variation, the eigenvectors (Tables 3 and 4 and reference [9]) are each dominated by a single displacement harmonic, with the contributions from other harmonics decreasing rapidly. It may therefore be expected that the interaction between the profile harmonic and the dominant displacement harmonic in each mode will be the most important.

Returning now to the above mentioned case where the profile contains a single harmonic, i, it may therefore be expected that the most important cases will be as follows. When the profile harmonic is even then $i = 2n$ or $2m$ is likely to be the most important (especially as this case relates to h rather than αh^3), with cases where $i = m \pm n$ and $3i = 2n$, $2m$ or $3i = n \pm m$ being of less importance, especially when m and n are significantly different from i. This is consistent with the results of Table 1 where, for example, $i = 4$ ($\phi = \pi$) leads to a relatively large split in the 2β mode progressively smaller splits in the 4β and 6β modes. When

the profile harmonic, i is odd the conditions $i = 2n$ or $2m$ and $3i = 2n$ or $2m$ can not be fulfilled. Therefore, non-zero integrals can only result from the combinations $i = m \pm n$ and $3i = n \pm m$. The most important of these is likely to be $i = m \pm n$ (since this is related to h) in the case where $m = 0$, $n = i$ or vice versa. This is consistent with the results presented in Table 2 where, for example, $i = 3$ ($\phi = \pi$) only produces a noticeable frequency split in the 3β mode.

When more than one profile harmonic is present, the combinations of profile and displacement harmonics which potentially give rise to non-zero contributions to the energy integrals increases rapidly. No attempt will be made here to give further detailed explanation. Suffice to say that the large number of possible combinations means that, in principle, only two or three low order profile harmonics have the capacity to couple with almost all the modes that are likely to be of practical engineering interest. The degree of interaction will often be very small but it is difficult to generalise and each specific case needs individual analysis. It is clear, however, that the strongest interaction will always arise between an even profile harmonic, say i, and the modes whose dominant displacement harmonic is $i/2$.

5. CONCLUSIONS

This paper reports a numerical study of the vibration of a thin ring with a rectangular cross-section and circumferential profile variation. Profile variations are represented, in the general way, by Fourier series functions. The method gives *quantitative* predictions of frequency splitting which are found to be in agreement with previously published *qualitative* results on frequency splitting patterns.

Numerical results have been presented for a number of example cases in which the inner and outer profiles are nominally circular with various superimposed harmonic variations in radius. For a ring with a single harmonic variation in profile, the effects of the harmonic number and of the amplitude and spatial phasing of the inner and outer surfaces have been investigated and the frequency splitting patterns have been noted. The effects of multiple harmonic variations in profile have also been investigated and the combinations of harmonics that cause frequency splitting have been investigated. The most important causes of frequency splitting have been identified and highlighted.

REFERENCES

1. R. S. Hwang, C. H. J. Fox and S. McWilliam 1999 *Journal of Sound and Vibration* **220**, 497–516. The in-plane vibration of thin rings with in-plane profile variations Part I: general background and theoretical formulation.
2. C. H. J. Fox 1990 *Journal of Sound and Vibration* **142**, 227–243. A simple theory for the analysis and correction of frequency splitting in slightly imperfect rings.
3. C. H. J. Fox 1988 *Proceedings of DGON Symposium on Gyro Technology Stuttgart, Germany*. Vibrating cylinder rate gyro: theory of operation and error analysis.
4. R. Perrin 1971 *Acustica* **25**, 69–72. Selection rules for the splitting of the degenerate pairs of natural frequencies of thin circular rings.

5. T. Charnley and R. Perrin 1973 *Acustica* **28**, 139–146. Perturbation studies with a thin circular ring.
6. T. P. Valkering and T. Charnley 1983 *Journal of Sound and Vibration* **86**, 369–393. Radial vibrations of eccentric rings.
7. R. F. Tonin and D. A. Bies 1979 *Journal of Sound and Vibration* **62**, 165–180. Free vibration of circular cylinders of variable thickness.
8. R. N. Wake *et al*. 1998 *Journal of Sound and Vibration* **214**, 761–770. Changes in the natural frequencies of repeated mode pairs induced by cracks in a vibrating ring.
9. R. S. Hwang 1997 *Ph.D. Thesis*, *University of Nottingham*, *UK*. Free vibrations of a thin ring having circumferential profile variations.
10. V. V. Novozhilov 1959 *The Theory of Thin Shells*. Grönigen, Holland: 1st edition.